ACS OMEGA

Open Access

http://pubs.acs.org/journal/acsodf

Article

Revealing the Mechanisms of Qilongtian Capsules in the Treatment of Chronic Obstructive Pulmonary Disease Based on Integrated Network Pharmacology, Molecular Docking, and *In Vivo* Experiments

Ying Xie,[#] Zhengyan Li,[#] Yiyao Liang, Tong Zhou, Xiaolin Yuan, Xuerong Su, Zhitong Zhang, Jiuba Zhang, Yi Wan, Lianlin Su, Tulin Lu, Xiaoli Zhao,* and Yi Fu*

Cite This: *ACS Omega* 2024, 9, 32455−32468

Read Online

ACCESS | Metrics & More | Article Recommendations | Supporting Information

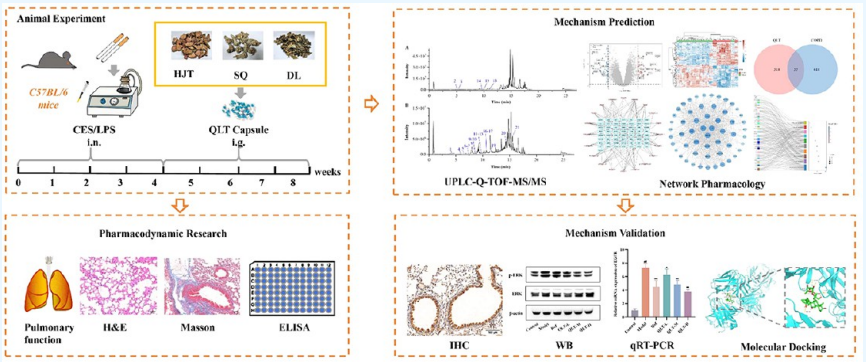

ABSTRACT: The Qilongtian capsule (QLT) is a Chinese patent medicine that has been approved for the treatment of chronic obstructive pulmonary disease (COPD). However, the precise pharmacodynamic material basis and molecular mechanism have not been well illustrated. In this study, we identified the effect of QLT on COPD through a cigarette smoke extract (CSE)/lipopolysaccharide (LPS) induced COPD mice model. The absorption of blood components in QLT were identified using ultrahigh performance liquid chromatography−quadrupole time-of-flight mass spectrometry (UPLC-Q-TOF-MS). Network pharmacology was used to predict the potential targets and therapeutic mechanisms of QLT, which were further validated using *in vivo* experiments and molecular docking. Pharmacodynamic studies revealed that QLT could ameliorate pulmonary function and pulmonary pathology, reduce collagen fiber accumulation, and attenuate inflammatory responses in mice with CSE/LPS induced COPD. A total of 21 components of QLT absorbed in the blood were detected. Network pharmacology analysis indicated that TNF, IL-6, EGFR, and AKT1 may be the core targets, mainly involving the MAPK signaling pathway. Besides, Sachaloside II, Ginsenoside Rh1, Ginsenoside F1, Rosiridin, and Ginsenoside Rf were the key compounds. Molecular docking results showed that the key components could spontaneously bind to EGFR and MAPK to form a relatively stable conformation. *In vivo* experiments revealed that QLT could suppress the activation of the EGFR/MAPK signaling pathway, thereby improving lung injury in mice with COPD. Overall, these findings provide evidence for the treatment of COPD with QLT.

1. INTRODUCTION

Chronic obstructive pulmonary disease (COPD) is a respiratory disease that mainly results from exposure to toxic particles and gases. It is characterized by an expiratory tract obstruction and recurrent symptoms of the respiratory system. Airway inflammation, oxidative stress, protease−antiprotease imbalance, and apoptosis are the commonly reported pathogenesis of COPD.[1−3] Moreover, the World Health Organization speculates that COPD will become the third-highest cause of mortality worldwide by 2030.[4,5]

Modern medicine mainly uses long-acting bronchodilators (LABD) and inhaled corticosteroids (ICS), including roflumilast, tiotropium bromide, and budesonide, for the treatment of COPD. The combination of ICS and LABD to form a double or triple therapy is commonly used as first-line treatment.[6−8] However, long-term use of bronchodilators or glucocorticoids can cause side effects such as arrhythmia,

Received: December 19, 2023
Revised: April 30, 2024
Accepted: July 5, 2024
Published: July 18, 2024

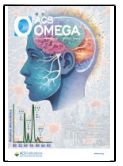

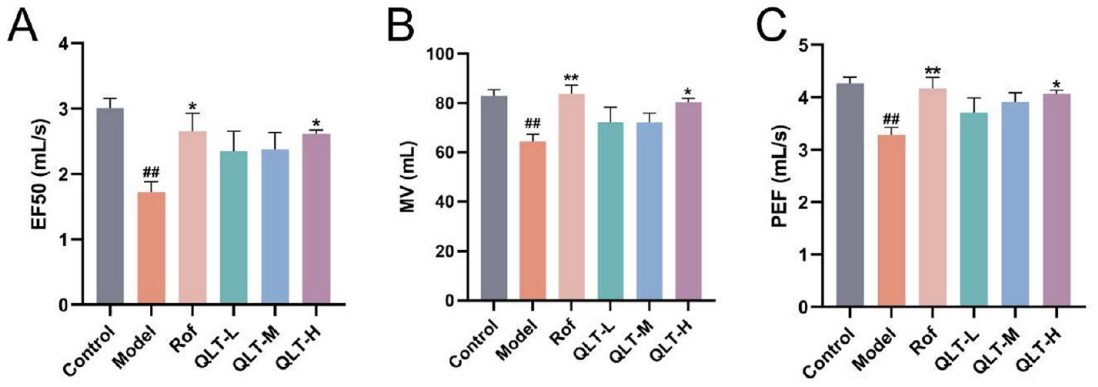

Figure 1. Effect of QLT on the pulmonary function. EF50 (A), MV (B), and PEF (C) were examined using unrestrained whole-body plethysmography. *$p < 0.05$ and **$p < 0.01$ vs the model group; $^{\#\#}p < 0.01$ vs the control group ($n = 6$).

metabolic disorders, and immune suppression.[9] Additionally, the treatment effect is not attainable in patients with stable COPD.[10−12] Compared with Western medicine, Chinese medicine has a long history of application, plays a vital role in the management of chronic respiratory diseases with fewer side effects, and can be used to prevent and control multiple targets and pathways. Thus, seeking the help of an herbal medicine may be a new strategy for treating COPD.

The Qilongtian capsule (QLT) is a clinical prescription developed by the Kunming Municipal Hospital of Traditional Chinese Medicine (Yunnan, China). It has been used in treating COPD in several hospitals in Yunnan since 2008 and has achieved ideal clinical efficacy. QLT was also approved by the Yunnan Provincial Emergency Approval Document for the prevention and control of COVID-19 (approval number 2020003A). QLT comprises three Chinese herbal medicines, namely, *Rhodiola crenulate* (Hongjingtian; HJT), *Pheretima aspergillum* (Dilong; DL), and *Panax notoginseng* (Sanqi; SQ), with the functions of tonifying Qi and strengthening healthy Qi, removing blood stasis and dredging collaterals, and eliminating phlegm and relieving asthma.[13] HJT is the sovereign drug and has been reported to have anti-inflammatory, immunomodulatory, antioxidant, and adaptogenic effects[14,15] with clinical efficacy in the treatment of COPD.[16,17] SQ, a minister drug, is widely used to prevent and treat various conditions. It has good effects in anti-inflammation,[18−20] antitumor capabilities,[21] promoting blood circulation and removing blood stasis,[22,23] immune regulation,[24] neuroprotection,[25] antioxidant capabilities,[26,27] and other aspects.[28] DL as a supplementary drug is recorded in the Shennong Materia Medica Classic, which has the effects of clearing heat and relieving fright, promoting circulation, and calming asthma and diuretic symptoms.[29] Owing to the regional characteristics of "plateau hypoxia, changeable climate, and numerous smokers", residents of the Yunnan-Guizhou plateau are prone to COPD. A randomized controlled clinical trial demonstrated that treatment with QLT had no significant effect on liver and kidney function (AST, ALT, BUN, Scr levels) and coagulation function (PT, APTT, TT, FIB) of patients with stable COPD. Besides, the levels of TGF-β1 and MMP-9, CAT score, symptom score, and total score reduced significantly, and the pulmonary function indices (FVC, FEV1, FEV1/FVC) increased significantly after treatment of patients with COPD with QLT.[30] Furthermore, pharmacological research has shown that QLT can ameliorate the oxidative stress balance by regulating the levels of Nrf2 and DJ-1, thereby exerting a certain therapeutic effect on rats with COPD.[31] The above research provides new insights into the protective effect of QLT in COPD.

The efficacy of QLT in treating diseases is thought to be linked to its multicomponent, multitarget, and multipathway effects. However, the effective components and mechanisms of action of QLT in treating COPD remain unclear. Hence, in order to explore the therapeutic effect of QLT, a mouse model of COPD induced by cigarette smoke extract (CSE)/lipopolysaccharide (LPS) was established. Next, the pharmacodynamic substances and molecular mechanisms were explored by using a combination of UPLC-Q-TOF-MS/MS and network pharmacology, which were further validated by using molecular docking and *in vivo* experiments. In conclusion, this study sets the stage for the further exploration of the mechanism of action of QLT against COPD in a clinical setting.

2. RESULTS

2.1. Effect of QLT on the Pulmonary Function in Mice with COPD. Airflow limitations are the hallmark features of COPD, which lead to a reduction in pulmonary function. Therefore, unrestrained pulmonary function was determined to evaluate the therapeutic effects of QLT on mice with COPD. The 50% vital capacity (EF50), minute ventilation (MV), and peak expiratory flow rate (PEF) after treatment with CSE/LPS decreased markedly in comparison with those in the control group ($p < 0.01$) and increased markedly after treatment with high-dose QLT (4.8 g/kg) and Rof (5 mg/kg) compared with those in the model group ($p < 0.05$ or $p < 0.01$) (Figure 1), suggesting that QLT could improve the pulmonary function that was damaged by CSE/LPS.

2.2. Effect of QLT on Pulmonary Histological Damage in Mice with COPD. H&E staining was used to determine the protective effects of QLT in pulmonary histological damage. As shown in Figure 2, the lung tissues of mice in the control group showed an unobvious airway inflammation around the bronchial epithelium, and the structures of the lung alveolar cavity were intact. However, mice exposed to CSE/LPS exhibited severe pathological changes. Bronchial inflammatory cell infiltration, thickening of the bronchial wall, expansion of the alveolar cavity, and thinning of the alveolar wall were observed in the model group. QLT (1.2, 2.4, and 4.8 g/kg) and Rof (5 mg/kg) treated mice exhibited an alleviation in CSE/LPS induced pathologic changes in the lungs compared with those in the model group. The improvement was more obvious

https://doi.org/10.1021/acsomega.3c10163
ACS Omega 2024, 9, 32455−32468

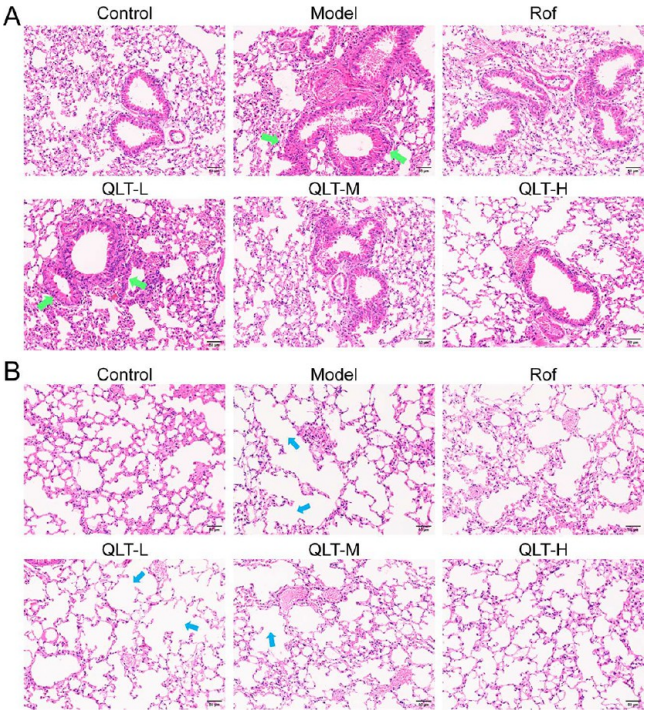

Figure 2. Effect of QLT on pulmonary histological damage in mice with COPD. Representative micrographs of H&E staining. (A) Peribronchial region. (B) Alveolar region. The green arrow represents thickening of the bronchial wall, and the blue arrow represents incomplete alveolar structure.

with an increase in QLT dosage. These results indicate that QLT ameliorated CSE/LPS induced pathological lesions in the lungs.

2.3. Effect of QLT on Collagen Deposition in Mice with COPD. Next, Masson's staining was used to determine the role of QLT in collagen deposition. As shown in Figure 3, CSE/LPS treatment induced fibrosis in the lung tissues of mice, and there was a significantly increased area of fibrosis compared with that in mice in the control group ($p < 0.01$). After QLT (1.2, 2.4, and 4.8 g/kg) treatment, the fibrotic area in the lung tissues reduced in a dose-dependent manner compared with that of mice in the model group ($p < 0.05$ or $p < 0.01$), indicating the inhibition of CSE/LPS induced fibrosis. The administration of Rof (5 mg/kg) also led to similar effects ($p < 0.01$). Therefore, QLT could ameliorate CSE/LPS induced accumulation of collagen fibers.

2.4. Effect of QLT on the Inflammatory Cytokines in Mice with COPD. The inflammatory response may interfere with the normal repair and defense mechanisms of the lung, resulting in emphysema and small-airway fibrosis. Thus, the inflammatory cytokine levels in the lung homogenate and serum were determined by ELISA. The results showed that after exposure to CSE/LPS, IL-1β and IL-6 levels in the lung and serum increased significantly compared with those in the control group ($p < 0.01$). However, the increments were attenuated after QLT (1.2, 2.4, and 4.8 g/kg) and Rof (5 mg/kg) intervention compared with those in model mice ($p < 0.05$ or $p < 0.01$) (Figure 4). Moreover, these levels decreased in a dose-dependent manner after treatment with QLT. These findings indicated that QLT could alleviate COPD by decreasing the inflammatory response.

2.5. UPLC-Q-TOF-MS/MS Analysis of Active Components of QLT. To explore the pharmacodynamic material basis of QLT in treating COPD, UPLC-Q-TOF-MS/MS was used to analyze the QLT components in the serum of mice after oral administration of QLT. A total of 74 compounds were identified and inferred from QLT, including 14 flavonoids, 16 saponins and terpenoids, three phenylpropanoids, 11 organic acids, and other components (Figure S1 and Tables S2 and S3). A total of 21 original constituents migrating to blood were identified, consisting of six flavonoids, 11 saponins, and four other components (Figure 5 and Tables 1 and S1).

2.6. Network Pharmacology Analysis of QLT in Treating COPD. Forty-five differentially expressed genes (DEGs) were upregulated, and 46 DEGs were downregulated (Figures 6A and 6B) in the Gene Expression Omnibus (GEO) database. Based on the SwissTargetPrediction database search, 375 targets predicted by 21 constituents were absorbed in the blood. Combining GEO, DisGeNET, and Genecards databases, 675 targets associated with COPD were collected. The components−targets network was constructed to further reveal the key components of QLT in treating COPD. This network comprised 396 nodes and 944 edges (Figure 6D), showing that

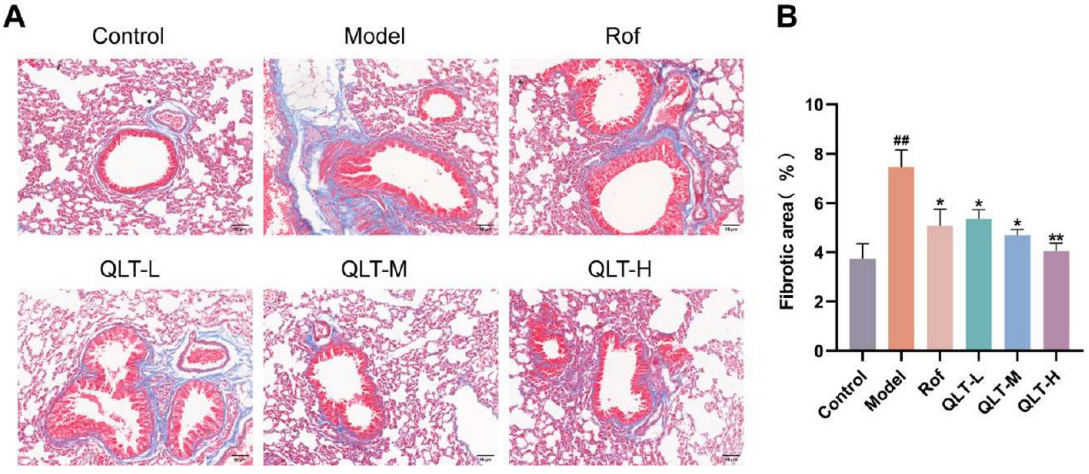

Figure 3. Effect of QLT on collagen deposition in mice with COPD. (A) Representative micrographs of Masson's staining. (B) Fibrotic areas were quantified using ImageJ software. *$p < 0.05$ and **$p < 0.01$ vs the model group; $^{\#\#}p < 0.01$ vs the control group ($n = 6$).

https://doi.org/10.1021/acsomega.3c10163
ACS Omega 2024, 9, 32455−32468

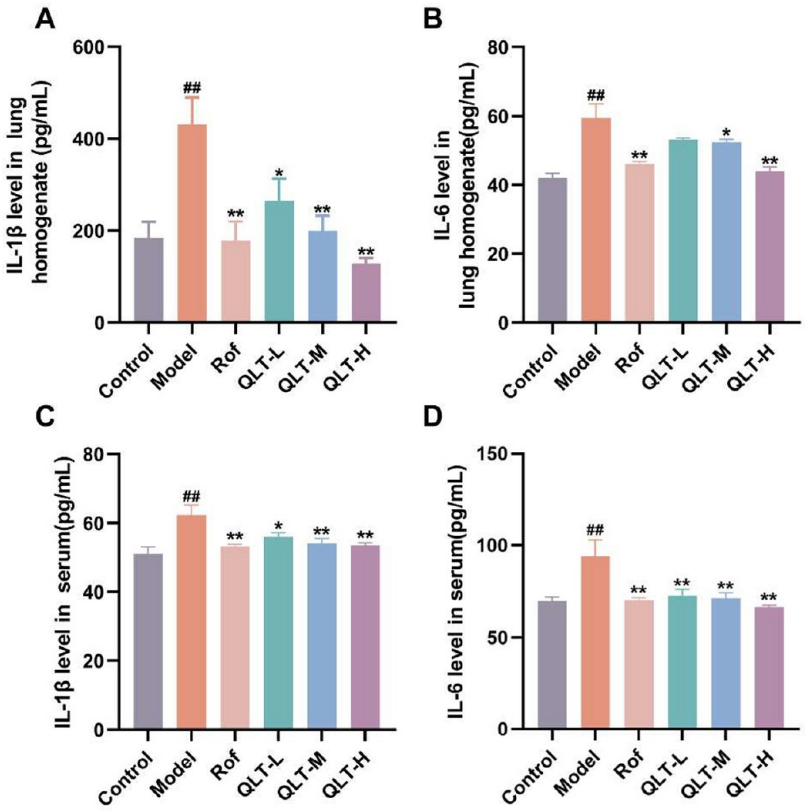

Figure 4. Effect of QLT on inflammatory cytokines levels. IL-1β (A) and IL-6 (B) levels in the lung homogenate and IL-1β (C) and IL-6 (D) levels in the serum. *$p < 0.05$ and **$p < 0.01$ vs the model; $^{\#\#}p < 0.01$ vs the control ($n = 6$).

multiple ingredients act on multiple targets; among them, Sachaloside II, Ginsenoside Rh1, Ginsenoside F1, Rosiridin, and Ginsenoside Rf were the top five nodes with higher betweenness centrality, closeness centrality, and degree and were thought to be the key compounds.

There were 57 overlapping targets between QLT and COPD that were acquired using the Venn diagram (Figure 6C). These targets were used to construct the protein−protein interaction (PPI) network (Figure 6E). The larger nodes represent a higher degree of and greater contribution to the intersection. The result showed that TNF, IL6, EGFR, AKT1, IFNG, HIF1A, STAT3, IL1B, CASP3, and MTOR, which have the highest degree, might be the core targets.

Besides, to reveal the possible signaling pathways of QLT to determine the therapeutic effect in COPD, Metascape was used to perform GO and KEGG analysis of the targets in the PPI network. It showed that the numbers of CC, MF, and BP were 58, 72, and 1257, respectively ($p < 0.05$, Figure 6F). According to the lowest p value, the top five BPs were positive regulation of MAP kinase activity, positive regulation of protein kinase B signaling, positive regulation of ERK1 and ERK2 cascades, positive regulation of gene expression, and negative regulation of the apoptotic process. The top five CCs were receptor complex, membrane raft, extracellular space, extracellular region, and plasma membrane. The top five MFs were endopeptidase activity, protein tyrosine kinase activity, cytokine activity, protein serine/threonine/tyrosine kinase activity, and protein kinase activity. After KEGG pathway analysis, a total of 167 signaling pathways were obtained ($p < 0.05$, Figure 6G). The top five signaling pathways are the EGFR, MAPK, PI3K-AKT, HIF-1, and TNF signaling pathways.

2.7. Molecular Docking. Based on network pharmacology results, compounds with the top five degree value in the components−targets network were screened, including Sachaloside II, Ginsenoside Rh1, Ginsenoside F1, Rosiridin, and Ginsenoside Rf. Thus, these compounds were docked with EGFR (PDB ID: 3G5X) and MAPK (PDB ID: 6ZWP) for further validation. The results revealed that the targets could spontaneously bind to the components to form a relatively stable conformation (the binding affinity was < −6 kcal/mol) (Table 2), indicating that these key compounds demonstrated good biological activity, which was consistent with the above results. The visualization results are shown in Figure 7.

2.8. Experimental Validation of the Molecular Mechanism. The MAPK signaling pathway may be a core pathway for the treatment of COPD based on KEGG enrichment analysis. The experimental results suggested that CSE/LPS significantly increased the phosphorylation levels of ERK, p38, and JNK compared with that in the control group ($p < 0.01$), but QLT treatment reversed this effect compared with that in the model group ($p < 0.05$) (Figures 8A−8F). Meanwhile, compared with the control group, the mRNA expression of ERK, p38MAPK, and JNK in the lung tissue of the model group showed a significant increase trend ($p < 0.01$). After QLT treatment, the expression of mRNA was significantly downregulated ($p < 0.05$ or $p < 0.01$) (Figures 8H−8J).

Immunohistochemistry results showed that the model group had significantly elevated levels of EGFR compared with those in the control group ($p < 0.01$). Interestingly, EGFR mRNA and protein expression were significantly inhibited in mice treated with QLT ($p < 0.05$ or $p < 0.01$) (Figures 8G, 8K, and 8L) compared with the observations in the model group.

https://doi.org/10.1021/acsomega.3c10163
ACS Omega 2024, 9, 32455−32468

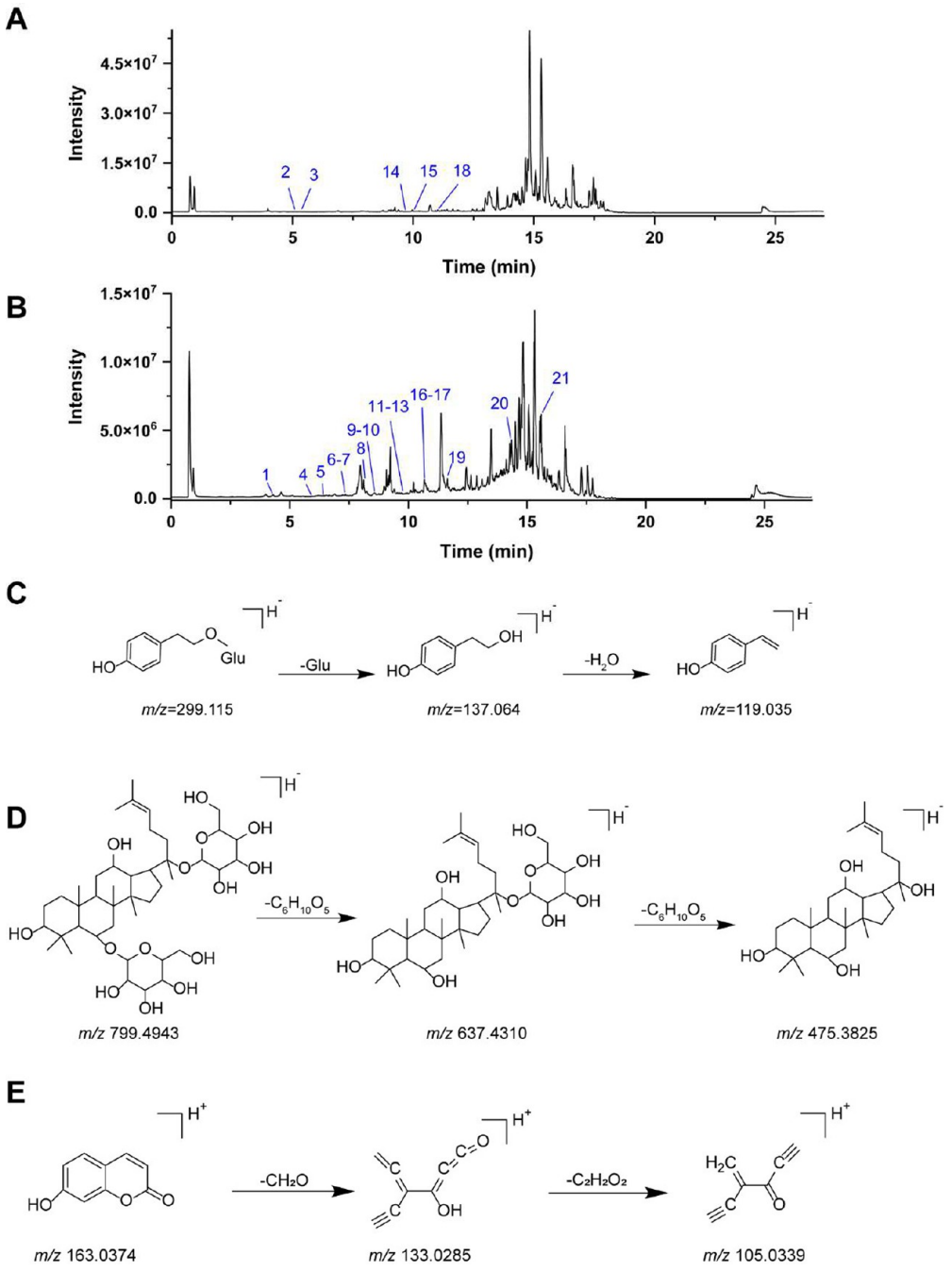

Figure 5. UPLC-Q-TOF-MS/MS to determine the absorption of blood components in QLT. Total ion chromatogram in positive ionization (A) and negative ionization (B) modes. The mass spectrometry cleavage pathways of representative components in positive/negative ion modes, including Salidroside (C), Ginsenoside Rg_1 (D), and 7-hydroxycoumarin (E).

3. DISCUSSION

QLT has been clinically proven to have favorable anti-COPD effects; however, its pharmacodynamic mechanism lacks in-depth studies. The pharmacological studies of QLT that have been reported so far usually use pulmonary hypertension models, which is not fully consistent with its clinical efficacy. Smoking is the most common risk factor for COPD, and CSE is the ideal stimulant to establish an animal model of COPD by using most of the ingredients in cigarette smoke. LPS is a cell wall component of Gram-negative bacteria; it can be used as a stressor to stimulate macrophages and epithelial cells, facilitate the release of inflammatory cytokines, and cause the acute exacerbation of COPD.[32] Therefore, we chose intranasal administration of CSE and LPS to establish a mouse model of COPD in this study. The model group mice showed slow weight gain, thickening of bronchial walls and infiltration of inflammatory cells, irregular enlargement of alveolar cavities, thinning and rupture of alveolar walls, and significant pathological damage to lung tissue, indicating the successful establishment of the COPD model.

Incomplete reversible airflow restriction is an essential physiological characteristic in the occurrence and development of COPD, and decreased pulmonary function can reflect the severity of airway obstruction.[33] Moreover, cigarette smoke inhalation, bacterial infections, or harmful gases may induce

https://doi.org/10.1021/acsomega.3c10163
ACS Omega 2024, 9, 32455−32468

Table 1. Identification of Original Constituents Migrating to Blood Based on UPLC-Q-TOF-MS/MS

no.	RT (min)	chemical formula	selected ion	mass-to-charge ratio (m/z)	theoretical mass (Da)	measured mass (Da)	error (ppm)	MS/MS	compund	source
1[a]	4.27	$C_{14}H_{20}O_7$	$[M-H]^-$	300.1209	299.1136	299.1146	3.2	137.0636, 119.0350, 101.0234, 89.0258	Salidroside	HJT
2	5.11	$C_{11}H_{20}O_6$	$[M+Na]^+$	248.126	271.1152	271.115	−0.7	203.0511, 165.0573, 97.1004	Crenulatin	HJT
3	5.31	$C_{14}H_{24}O_7$	$[M+Na]^+$	304.1522	327.1416	327.1412	−1.3	165.0859, 98.9852	Creoside I	HJT
4	5.96	$C_{14}H_{26}O_7$	$[M+COOH]^-$	306.1679	351.165	351.1678	8.1	304.8562, 161.0030, 101.0247	Creoside II	HJT
5	6.4	$C_9H_8O_3$	$[M-H]^-$	164.0473	163.0401	163.0395	−3.9	119.0520, 117.0347, 93.0353	*p*-coumaric acid	HJT, SQ
6	7.43	$C_{16}H_{30}O_8$	$[M-H]^-$	350.1941	349.1868	349.1863	−1.3	161.0016, 141.0921	Rhodioloside D	HJT
7	7.54	$C_{16}H_{28}O_7$	$[M+COOH]^-$	332.1835	377.1806	377.1819	3.3	149.0239, 103.4700	Rosiridin	HJT
8	8.1	$C_7H_6O_3$	$[M-H]^-$	138.0317	137.0244	137.0254	6.9	108.0223, 93.0366	*p*-hydroxybenzoic acid	HJT
9[a]	8.53	$C_{42}H_{72}O_{14}$	$[M+COOH]^-$	800.4922	845.4893	845.4901	0.9	799.4943, 637.4310, 475.3825	Ginsenoside Rg_1	SQ
10	8.66	$C_{42}H_{72}O_{14}$	$[M+COOH]^-$	800.4922	845.4893	845.4933	4.7	799.4904, 637.4341, 475.3849	Ginsenoside Rf	SQ
11	9.65	$C_{19}H_{36}O_{10}$	$[M-H]^-$	424.2309	423.2236	423.2246	2.5	291.1802, 113.0247, 101.0261	Rhodiooctanoside	HJT
12	9.65	$C_{22}H_{38}O_{12}$	$[M-H]^-$	494.2363	493.2291	493.2311	4.2	447.2233, 191.0564, 149.0462	Rhodioloside C	HJT
13	9.66	$C_{21}H_{36}O_{10}$	$[M-H]^-$	448.2309	447.2236	447.2245	2.1	301.0381, 161.0008, 135.0460	Kenposide A	HJT
14	9.67	$C_{21}H_{34}O_{10}$	$[M+H]^+$	446.2152	447.2225	447.222	−1.1	343.0161, 315.1789, 207.0326, 147.0650	Sachaloside II	HJT
15	10.03	$C_9H_6O_3$	$[M+H]^+$	162.0317	163.039	163.0391	0.8	117.0567, 107.0498, 91.0541	7-hydroxycoumarin	HJT
16	10.88	$C_{42}H_{72}O_{13}$	$[M+COOH]^-$	784.4973	829.4944	829.4977	4	783.4899, 475.3812	Ginsenoside Rg_2	SQ
17	10.98	$C_{36}H_{62}O_9$	$[M+COOH]^-$	638.4394	683.4365	683.4392	4	475.3805, 475.3805	Ginsenoside F1	SQ
18	10.93	$C_{21}H_{20}O_{11}$	$[M+Na]^+$	448.1006	471.0898	471.0898	−7.3	409.0483, 383.0637, 339.0402, 131.0864	Rhodionin	HJT
19	11.57	$C_{36}H_{62}O_9$	$[M+COOH]^-$	638.4394	683.4365	683.4384	2.8	637.4341, 475.3849, 161.0470, 113.0247	Ginsenoside Rh1	SQ
20	14.36	$C_{17}H_{26}O_3$	$[M-H]^-$	278.1882	277.1809	277.1827	6.6	233.1925, 205.1622, 175.7251	Panaxytriol	SQ
21	15.68	$C_{16}H_{28}O_8$	$[M-H]^-$	348.1784	347.1711	347.1732	5.9	301.1694, 285.1367, 217.0746	Rhodioloside A	HJT

[a]Means the compositions identified by comparison with the reference substance.

the stimulation of inflammatory cells and the release of multiple inflammatory mediators (IL-6, IL-1β), which, in turn, cause a sustained cascade of the inflammatory response, mucus hypersecretion, small airway fibrosis, and lung tissue injury.[34−37] In addition, fibrosis observed predominantly around the small airways is associated with decreased lung function in patients with COPD.[38] Interestingly, we found that QLT effectively increased the pulmonary function index EF50, MV, and PEF; relieved pulmonary inflammatory responses by suppressing the levels of IL-1β and IL-6 released in the serum and lung tissue; and reversed pathological changes and peribronchial collagen accumulation in the lung tissues of mice with CSE/LPS induced COPD.

UPLC-Q-TOF-MS/MS identified a total of 21 prototype components, mainly saponins and flavonoids. Ginsenoside alleviates the cigarette smoke induced pulmonary epithelial−mesenchymal transition in both COPD rats and HBE cells via inhibition of the TGF-β1/Smad pathway.[39,40] Rhodiola glycoside inhibits the production of proinflammatory cytokines and M1 polarization of alveolar macrophages in mouse serum and lungs induced by cigarette smoke. In addition, the administration of Rhodiola glycoside significantly inhibits the protein levels of the MAPK/NF-κB pathway.[41,42] The KEGG results indicated that MAPK is a core signaling pathway for treating COPD with QLT, which was predicted using network pharmacology. The MAPK pathway can be activated when exposed to cigarette smoke, LPS, or cytokines.[43] MAPK signaling is important in regulating COPD-associated phenotypes, including airway inflammation, mucus secretion, and airway remodeling.[44,45] It has been reported that phosphorylation of ERK1/2 and p38 MAPK in the MAPK pathway is a key step that mediates the expression of IL-1β and TNF-α.[46] EGFR can be activated by cigarette smoke and is involved in airway remodeling, chemokine overexpression, pulmonary fibrosis, mucin hypersecretion, and goblet cell metaplasia.[47−49] Goblet cell hypertrophy and hyperplasia are features observed in cigarette smokers that lead to epithelial mucin hypersecretion. The results from experimental validation indicated that the phosphorylation of the EGFR/MAPK signaling pathway that increased in mice with COPD could be suppressed after the administration of QLT (Figure 9). Furthermore, molecular docking revealed that the key compounds were relatively stable in combination with the core targets. Overall, these results contribute to further exploration of the molecular mechanism of QLT to provide further support for the use of QLT in treating COPD. However, the active ingredients of QLT in the treatment of COPD have not been experimentally verified. Further exploration is needed to provide evidence for the development of the QLT prescription.

https://doi.org/10.1021/acsomega.3c10163
ACS Omega 2024, 9, 32455−32468

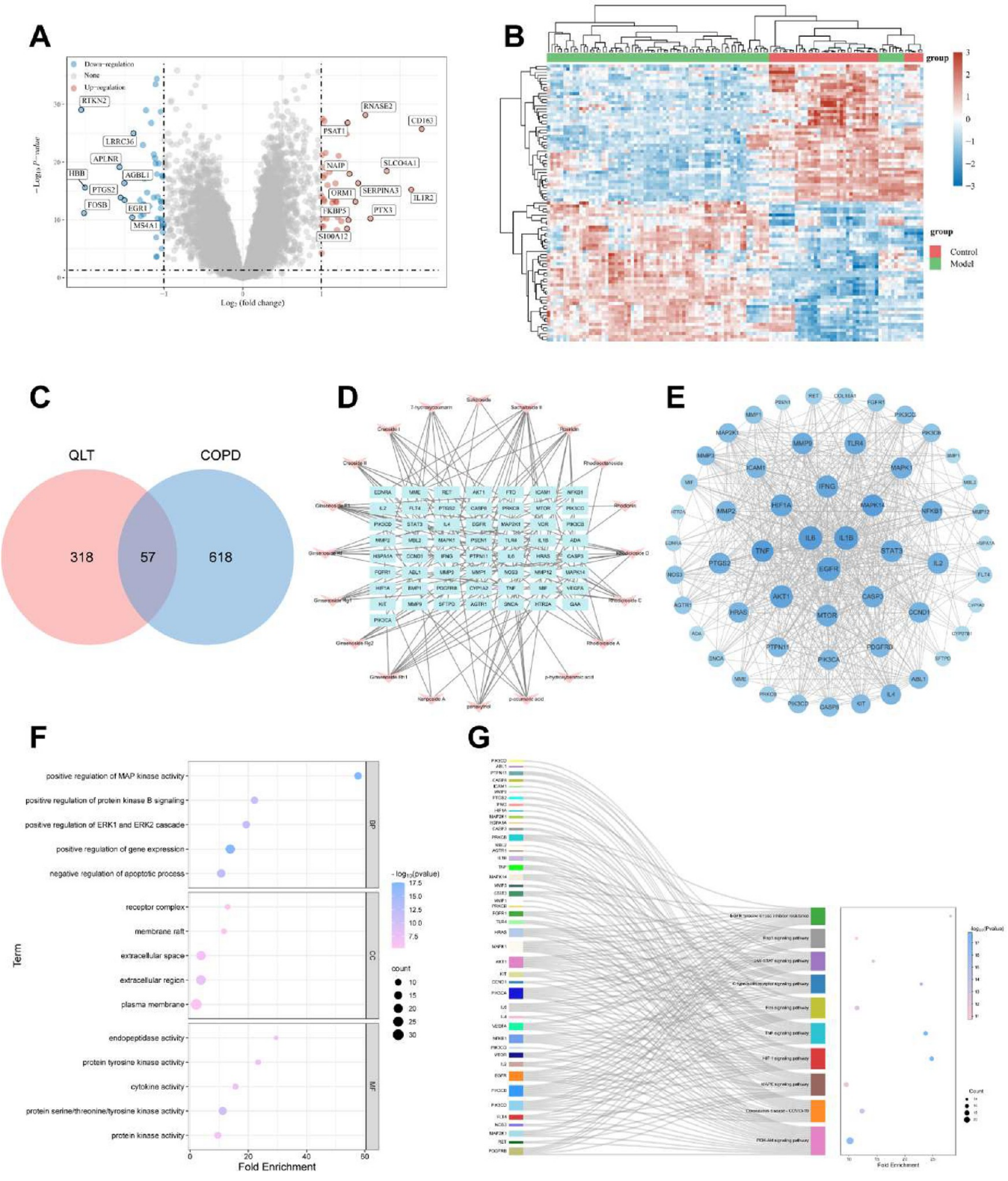

Figure 6. Network pharmacology analysis. (A) Volcano map of DEGs in the lungs between COPD patients and healthy controls. (B) Heatmap of DEGs between COPD patients and healthy controls. (C) Venn diagram. (D) Compounds−targets network. The blue rectangles represent targets; the pink arrows represent compounds. (E) PPI network. (F) GO enrichment. (G) KEGG enrichment.

4. CONCLUSIONS

QLT could alleviate airflow limitation, pulmonary histological damage, collagen deposition, and inflammatory responses in mice with CSE/LPS induced COPD. UPLC-Q-TOF-MS/MS and network pharmacology were used to predict the potential pharmacodynamic substances and molecular mechanisms of QLT in treating COPD. Sachaloside II, Ginsenoside Rh1, Ginsenoside F1, Rosiridin, and Ginsenoside Rf may be the key pharmacodynamic substances in this process. Verification of

https://doi.org/10.1021/acsomega.3c10163
ACS Omega 2024, 9, 32455−32468

Table 2. Binding Affinity (kcal/mol) between Targets and Components

component	EGFR		MAPK	
	binding affinity	binding residues	binding affinity	binding residues
Sachaloside II	−8.1	Tyr	−8.2	Arg, Lys, Asp, Ile, Phe
Ginsenoside Rh1	−7.9	Gln, Asn, Asp, Ala	−7.5	Thr, Val
Ginsenoside F1	−7.9	Leu, Asn, Asp	−7.7	Leu, Val
Rosiridin	−6.8	Glu, Ala	−6.5	Met, His
Ginsenoside Rf	−8.3	Gln, Gly, Asn, Thr, Trp	−7.9	Phe

the prediction using *in vivo* experiments and molecular docking revealed that the mechanism of action may be closely related to the inhibition of the EGFR/MAPK signaling pathway. Therefore, QLT may be a promising therapeutic agent to treat COPD. Our study serves as an important reference to further elucidate the pharmacological mechanism and promote the clinical use of QLT.

5. MATERIALS AND METHODS

5.1. Chemicals and Reagents. Qilongtian capsules were provided by Kunming Municipal Hospital of Traditional Chinese Medicine. Enzyme-linked immunosorbent assay (ELISA) kits for interleukin (IL)-6 and IL-1β were obtained from YiFeiXue Biotechnology (Nanjing, China). TRIzol reagent was obtained from Invitrogen Life Technologies (Carlsbad, USA). The Hifair V one-step RT-gDNA digestion SuperMix for quantitative polymerase chain reaction (qPCR) kit, radio-immunoprecipitation assay (RIPA), and bicinchoninic acid (BCA) protein quantification kit were obtained from Yeasen Biotechnology Co., Ltd. (Shanghai, China). TORO-Green qPCR Master Mix kits were purchased from Toroivd Technology Co., Ltd. (Nantong, China). Anti-EGFR rabbit pAb was obtained from Servicebio Biotechnology Co., Ltd. (Wuhan, China). Antibodies of ERK1/2 rabbit pAb, phospho-ERK1/2 (Tyr204/Tyr187) rabbit pAb, p38 (5A1) mouse mAb, phospho-p38 (Thr180/Tyr182) rabbit pAb, JNK rabbit mAb, phospho-JNK (Thr183) rabbit pAb, and β-actin (8F10) mouse mAb were purchased from Zen Biotechnology Co., Ltd. (Chengdu, China). Polyvinylidene fluoride (PVDF) membranes were obtained from PALL Life Company (New York, USA). Ultrapure water was obtained using a Milli-Q water purification system (Millipore, Bedford, USA). Phosphate buffered saline was purchased from KeyGEN Biotechnology Co., Ltd. (Nanjing, China). Acetonitrile (MS-grade) was purchased from Merck (Darmstadt, Germany). LPS and formic acid (MS grade, 98% purity) was purchased from Sigma-Aldrich (Saint Louis, USA). Cigarettes were purchased from China Tobacco Hunan Industrial Co., Ltd. (Hunan, China). Other reagents and chemicals were all of analytical grade and purchased from commercial reagent companies.

5.2. Preparation and Quality Control of QLT. QLT is composed of HJT, DL, and SQ in a 10:5:2 ratio and was provided by Kunming Municipal Hospital of Traditional Chinese Medicine. The raw medicinal materials were boiled with 10 times their volume of water (w/v) twice for 2 h each. The extracts were filtered, concentrated, and dried to obtain the QLT extract. Then, 70% ethanol was used as a wetting agent, followed by granulation, drying, and filling of capsules.

5.3. Preparation of CSE. Each cigarette contained 10 mg of tar, 1 mg of nicotine, and 13 mg of carbon monoxide. While burning, the smoke from one cigarette was drawn into 1 mL of PBS using a vacuum pump, and the dissolved smoke was filtered through a 0.22 μm filter. The CSE was freshly prepared for each experiment.

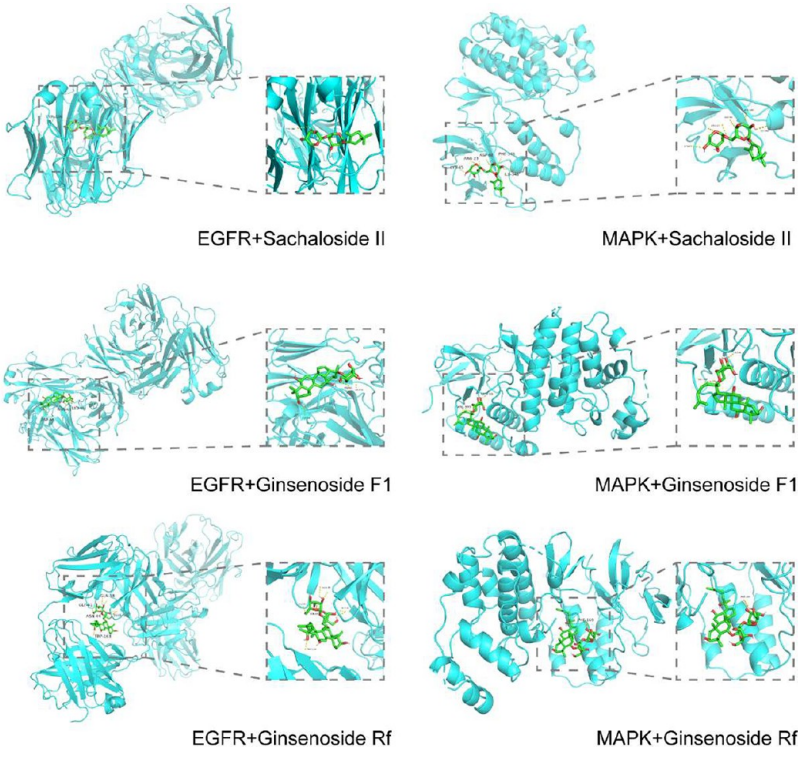

Figure 7. Partial 3D digital model of molecular docking between compounds and proteins.

https://doi.org/10.1021/acsomega.3c10163
ACS Omega 2024, 9, 32455−32468

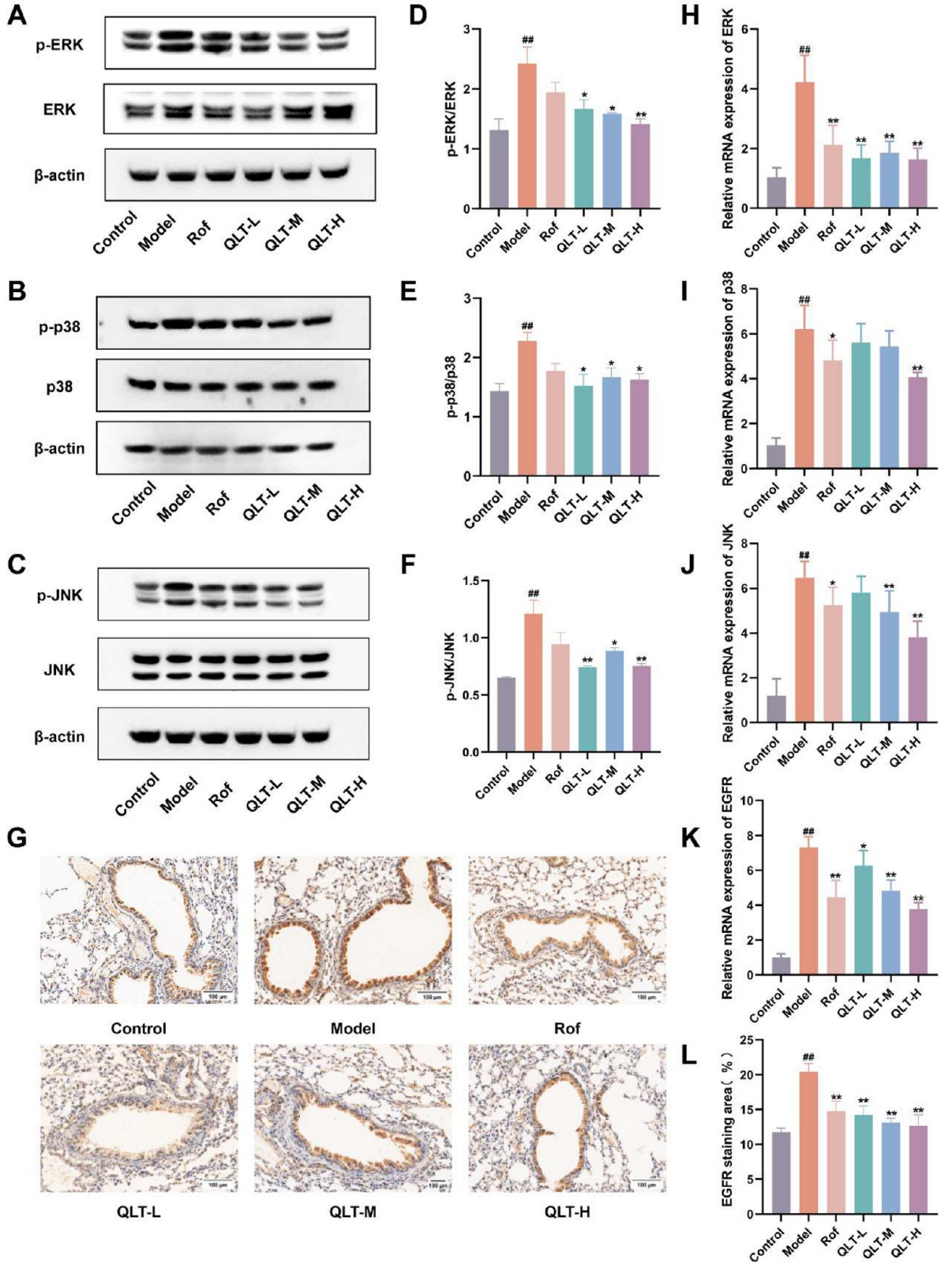

Figure 8. Experimental validation of the molecular mechanism. (A–F) Western blotting of p-ERK, ERK, p-p38, p38, p-JNK, and JNK using the lung tissues of mice (n = 3). (G) Representative micrographs of EGFR in the immunohistochemical assay. (H–K) qRT-PCR to determine the relative mRNA expression of ERK, p38MAPK, JNK, and EGFR in the lung tissues of mice (n = 6). (L) EGFR staining areas were quantified using ImageJ software (n = 6). Immunohistochemistry images were taken at ×400 magnification (scale bar: 50 μm). *p < 0.05 and **p < 0.01 vs the model; $^{\#\#}p$ < 0.01 vs the control.

5.4. Animal Studies. A total of 36 male C57BL/6 mice at 6 weeks of age (18–22 g) were purchased from Jiangsu Huachuang Xinnuo Pharmaceutical Technology Co., Ltd. (Taizhou, China). The mice were reared in a standard

https://doi.org/10.1021/acsomega.3c10163
ACS Omega 2024, 9, 32455−32468

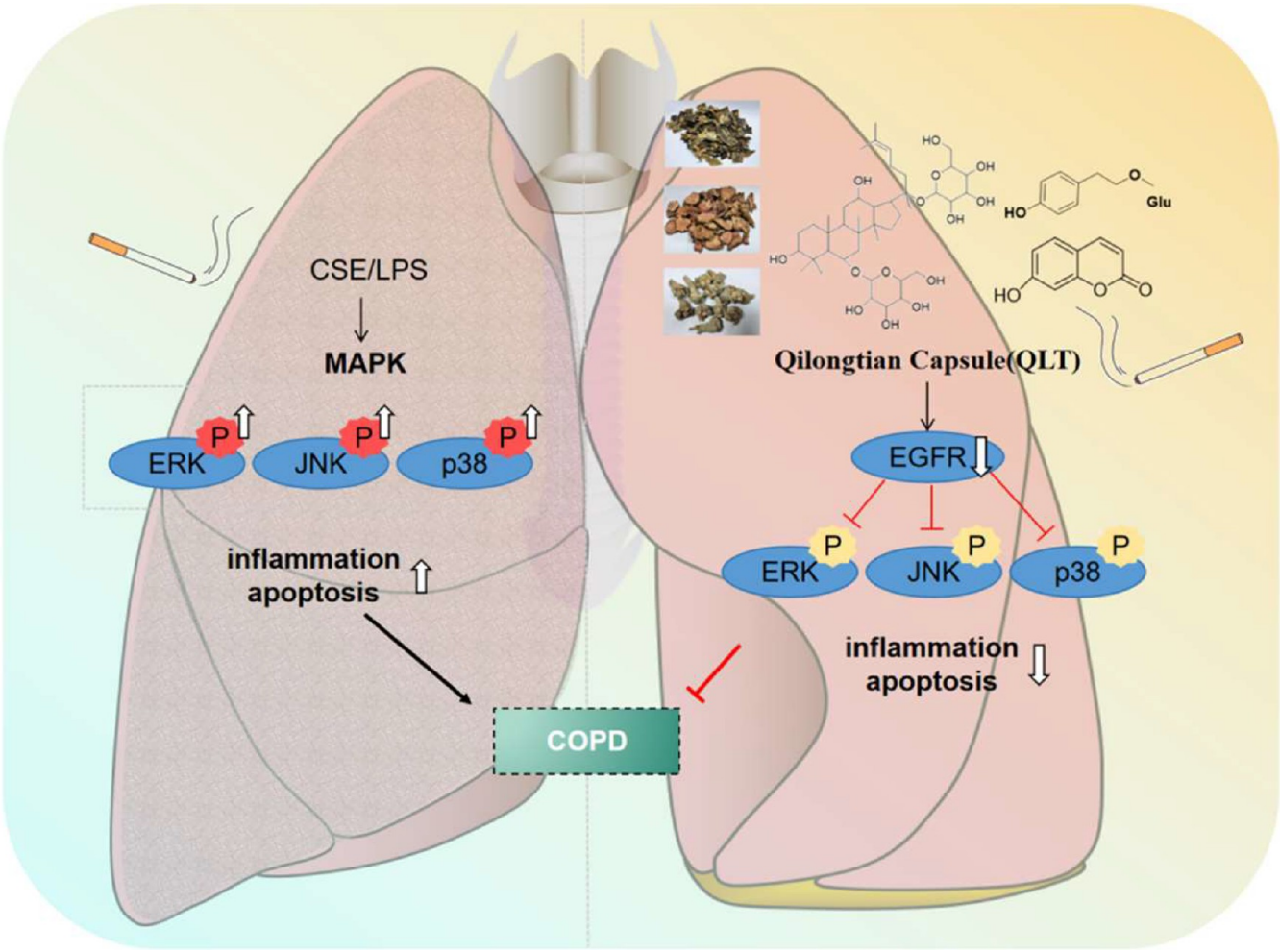

Figure 9. Molecular mechanisms. CSE/LPS stimulation can promote the activation of the MAPK pathway, thereby promoting the development of COPD, while QLT can downregulate the expression of EGFR, thereby inhibiting MAPK pathway activity and hindering the development of COPD.

environment of 22−25 °C and 60% humidity and subjected to a 12/12 h light/dark cycle with free access to food and water.

After 1 week of adaptive feeding, the mice were randomly divided into the following six groups (n = 6 mice/group): (1) negative control group (control); (2) COPD model group (model); (3) positive control group with roflumilast (Rof, 5 mg/kg); (4) QLT low-dose group (QLT-L, 1.2 g/kg); (5) QLT middle-dose group (QLT-M, 2.4 g/kg); and (6) QLT high-dose group (QLT-H, 4.8 g/kg). According to the conversion formula, 1.2 g/kg for each mouse daily was equivalent to clinical usage in humans. Therefore, we chose 1.2, 2.4, and 4.8 g/kg as the low, middle, and high doses of the drug, respectively, for administration. We referred to the modeling method reported in the literature and adjusted the modeling dose according to our pretest. Except those in the negative control group, all other experimental mice with COPD were intranasally administered 25 μL of CSE once daily; 10 μL of LPS (1 mg/mL) was intranasally administered to each mouse twice a week. An equal volume of PBS was intranasally administered to the mice in the control group. After infection with CSE/LPS for 4 weeks, Rof and QLT dissolved in distilled water were gavaged intragastrically to mice in the Rof, QLT-L, QLT-M, and QLT-H groups once daily for 4 weeks. At this time, equal amounts of distilled water were administered orally to mice in the control and model groups.

Specific pathogen-free-grade male Sprague−Dawley rats (200 ± 20 g) were purchased from the Hangzhou Medical College. The rats were allowed to acclimate for 1 week before the experiment. All rats were housed at ambient temperature (20 ± 2 °C), humidity (60 ± 5%), and light/dark cycle (12 h).

Blank serum was taken as a backup before administration. The QLT aqueous solution was intragastrically administered to the rats (n = 6) at 4.1 g/kg/day for 3 consecutive days. Medicated serum was collected after the last oral administration at 1 h and then centrifuged (0.9 × g for 10 min at 4 °C) and stored at −80 °C.

The animal protocols were approved and conducted by the Guide for the Care and Use of Laboratory Animal Center in Nanjing University of Chinese Medicine (approval number 202206A026). All procedures were in accordance with the Guide for the Care and Use of Laboratory Animals (National Institutes of Health).

5.5. Pulmonary Function Test. The EF50, MV, and PEF were measured on the day before the end of the animal experiment using whole-body plethysmography (Buxco, America).

5.6. Sample Collection. Before execution, blood was extracted from the eyeballs. Blood samples were allowed to

https://doi.org/10.1021/acsomega.3c10163
ACS Omega 2024, 9, 32455−32468

stand for 120 min and centrifuged at 1.2 × *g* for 10 min to obtain the serum, which was stored at −20 °C until further analysis. After execution, lung tissues were removed and divided into three parts. One part was used for preparing the lung homogenate. The lung tissues were homogenized with precooled PBS (w/v = 1:9) and centrifuged at 2.4 × *g* for 10 min at 4 °C; the lung homogenate was collected and stored at −20 °C. The other part was fixed in 4% paraformaldehyde, and the remaining lung tissues were stored at −80 °C.

5.7. UPLC-Q-TOF-MS/MS Analysis. First, 200 μL of serum was taken, and then 4 times the volume of acetonitrile was added and vortexed for 3 min. The solution was centrifuged at 4 °C and 18.8 × *g* for 10 min. The supernatant was blown into liquid nitrogen and dissolved again with 200 μL of acetonitrile.

UPLC-Q-TOF-MS/MS analysis was conducted by using a Shimadzu ExionLC system and Sciex ZenoTOF 7600 mass spectrometer (AB SCIEX, USA). An ACQUITY UPLC BEH C_{18} column (1.7 μm, 2.1 × 100 mm) was used; 3 μL was used as the injection volume, 40 °C was used as the chromatographic temperature, and 0.3 mL/min was used as the flow rate. The mobile phase consisted of (A) 0.1% formic acid in water and (B) methanol. The elution gradient was as follows: 0−2 min, 5% B; 2−12 min, 5∼50% B; 12−13 min, 50∼68% B; 13−18 min, 68∼95% B; 18−23 min, 95% B; 23−24 min, 95∼5% B; 24−28 min, 5% B.

The mass spectrum operating parameters were set as follows: ion spray voltage, 5500 eV; source temperature, 550 °C; collision energy, 45/−45 V; declustering potential, 80/−80 V. Data acquisition was performed using an Analyst TF workstation (version 1.6, AB SCIEX). The TOF MS scan range was *m*/*z* 80−2000.

5.8. Identification of Compounds. The compound database of QLT, including chemical name, molecular formula, molecular weight, and secondary fragments of the three herbal medicines, was established based on a literature search in PubMed and the Chinese National Knowledge Infrastructure. By comparing the mass spectrum data imported into Peakview 1.2 software with the compounds' information in the compound database of QLT, the components with mass errors of <10 ppm were identified and further verified using the MOL file.

5.9. Network Pharmacological Analysis of QLT. The compounds in QLT identified using UPLC-Q-TOF-MS/MS were imported into SwissTargetPrediction (http://www.swisstargetprediction.ch/) databases for target prediction. Among them, the targets in SwissTargetPrediction with probabilities >0.1 were selected.

The targets related to COPD were summarized using the GEO (http://www.ncbi.nlm.nih.gov/geo), DisGeNET (https://www.disgenet.org/), and Genecards (https://www.genecards.org/) databases. The microarray data GSE151052 from GEO was downloaded to analyze DEGs between lung samples of COPD patients and healthy controls, which were screened using the Bioconductor/R limma 3.4.2 software package with a *p* value of <0.05 and a $|\log_2 FC|$ of >1. Furthermore, the targets with a relevance score of >40 in the Genecards database and the targets with a score gda of >0.02 in the Genecards database were selected and combined with the targets gathered from GEO data sets.

The components and disease overlap targets are considered candidate targets for QLT in treating COPD, as shown in the Venn diagram. A PPI network was constructed using STRING (https://cn.string-db.org/) and Cytoscape 3.7.2 software with overlap targets. Next, the degree of the PPI network was analyzed to select the core targets.

The compounds and overlap targets were input into Cytoscape 3.7.2 to establish a compound−targets network, and the key components were screened using network topology parameters.

The overlap targets were submitted to the Metascape (https://metascape.org/) database to conduct GO and KEGG pathway enrichment analysis.

5.10. Molecular Docking. The 3D structure files of targets (receptors) were acquired from PDB (https://www.rcsb.org/), and the SDF files of compounds (ligands) were obtained from PubChem. The organic elements and solvents of the receptors were removed by PyMOL, and the SDF files of ligands were transformed into MOL2 files by using ChemDraw 3D 20.0. The ligands and receptors were imported into AutoDockTools 1.5.7 and converted into PDBQT format files. AutoDock Vina was used for molecular docking, and PyMOL was used to visualize the docking results.

5.11. Measurement of Inflammatory Cytokines Using ELISA. IL-6 and IL-1β levels in the lung homogenate and serum were measured using ELISA kits, and the manufacturer's instructions and operation methods were strictly followed.

5.12. H&E and Masson's Staining. Lung tissues were removed from 4% paraformaldehyde after 24 h of fixing. They were dehydrated with alcohol, embedded in paraffin blocks, and cut into 5 μm thick slices. Staining was performed using H&E and Masson's staining kits. Photographs were taken using a microscope (200×; PerkinElmer, America). The fibrotic area observed after Masson's staining was quantified using ImageJ software.

5.13. Western Blotting. RIPA lysis buffer was used to lyse the lung tissues, and a BCA protein assay kit was used to determine protein concentrations after centrifugation. SDS-PAGE and PVDF membranes were used for electro-transfer. After treatment with blocking fluid, the membranes were incubated with primary antibodies (1:1000) and secondary antibodies (1:2500). Lastly, the bands were visualized using the ECL reagent and quantified using ImageJ software.

5.14. Immunohistochemistry. The lung tissues embedded in paraffin were cut, dewaxed, dehydrated, and incubated in a citrate antigen retrieval solution for antigen repair. After inhibiting endogenous peroxidase activity and blocking with serum albumin, the slices were incubated with rabbit EGFR primary antibodies and later incubated with a secondary antibody bound to HRP. The sections were stained with a DAB substrate kit, and the nuclei were counterstained with hematoxylin. Digital photos were captured using a microscope (400×; PerkinElmer, America). EGFR expression in tissues was analyzed using ImageJ software.

5.15. qRT-PCR. Total RNA from lung tissues was extracted using a TRIzol reagent and reverse-transcribed into cDNA using Hifair V one-step RT-gDNA digestion SuperMix for qPCR kits. The samples were analyzed with TOROGreen qPCR Master Mix kits using LightCycler 96 (Roche, Indiana, USA). The operation methods of the kits were followed according to the manufacturer's instructions. Glyceraldehyde-3-phosphate dehydrogenase (GAPDH) was chosen as the control. The $2^{-\Delta\Delta Ct}$ method was used to determine the fold change difference between the experimental and calibration samples. The primer sequences are listed in Table 3.

https://doi.org/10.1021/acsomega.3c10163
ACS Omega 2024, 9, 32455−32468

Table 3. Primer Sequences in qPCR

gene	primer	primer sequences (5′ → 3′)
ERK	forward	AGTGTACAAGGGCCGATTGA
ERK	reverse	GTACCCAGCTTTCAGGGTCT
P38MAPK	forward	TCACTCCAGCTACGTTGTGT
P38MAPK	reverse	GTTCAGGTGCTCTGTTCGTC
JNK	forward	TCACCTGTGTCCCTCAGTTC
JNK	reverse	CCTGTCCTGTCAGTGTCCTT
EGFR	forward	AAAGGCAGCCACCAAATGAG
EGFR	reverse	GGCTTGGCTTCTTTGGGAAA
GAPDH	forward	ACCCCAGCAAGGACACTGAGCAAG
GAPDH	reverse	GGCCCCTCCTGTTATTATGGGGGT

5.16. Statistical Analysis. GraphPad Prism 9.0 was used for data analysis. Experimental data are expressed as the mean ± SEM and evaluated using ANOVA. $p < 0.05$ was considered statistically significant.

■ ASSOCIATED CONTENT

Supporting Information

The Supporting Information is available free of charge at https://pubs.acs.org/doi/10.1021/acsomega.3c10163.

The classification of QLT components migrating to blood, UPLC-Q-TOF-MS/MS to determine the chemical composition of QLT, identification of chemical components of QLT based on UPLC-Q-TOF-MS/MS, the classification of QLT components, HPLC diagram of QLT extract, and the content of the major active ingredients in QLT (PDF)

■ AUTHOR INFORMATION

Corresponding Authors

Xiaoli Zhao − *School of Pharmacy, Nanjing University of Chinese Medicine, Nanjing 210046, China*; orcid.org/0009-0002-1276-5134; Email: Leah_zhao@njucm.edu.cn

Yi Fu − *Department of Pharmacy, Kunming Municipal Hospital of Traditional Chinese Medicine, Kunming 650011, China*; Email: fukeyi_27@163.com

Authors

Ying Xie − *School of Pharmacy, Nanjing University of Chinese Medicine, Nanjing 210046, China*

Zhengyan Li − *Department of Pharmacy, Kunming Municipal Hospital of Traditional Chinese Medicine, Kunming 650011, China*

Yiyao Liang − *School of Pharmacy, Nanjing University of Chinese Medicine, Nanjing 210046, China*

Tong Zhou − *School of Pharmacy, Nanjing University of Chinese Medicine, Nanjing 210046, China*

Xiaolin Yuan − *School of Pharmacy, Nanjing University of Chinese Medicine, Nanjing 210046, China*

Xuerong Su − *School of Pharmacy, Nanjing University of Chinese Medicine, Nanjing 210046, China*

Zhitong Zhang − *School of Pharmacy, Nanjing University of Chinese Medicine, Nanjing 210046, China*

Jiuba Zhang − *School of Pharmacy, Nanjing University of Chinese Medicine, Nanjing 210046, China*

Yi Wan − *School of Pharmacy, Nanjing University of Chinese Medicine, Nanjing 210046, China*

Lianlin Su − *School of Pharmacy, Nanjing University of Chinese Medicine, Nanjing 210046, China*

Tulin Lu − *School of Pharmacy, Nanjing University of Chinese Medicine, Nanjing 210046, China*

Complete contact information is available at: https://pubs.acs.org/10.1021/acsomega.3c10163

Author Contributions

#Y.X. and Z.L. contributed equally to this work.

Notes

The authors declare no competing financial interest.

■ ACKNOWLEDGMENTS

The study was supported by the National Natural Science Foundation of China (82274374 and 82260924), the Basic Research Program of Yunnan Provincial Department of Science and Technology, Joint Special Project of Traditional Chinese Medicine (202101AZ070001-275), and the Yunnan Province Traditional Chinese Medicine Joint Youth Project (2019FF002(-087)).

■ ABBREVIATIONS

Akt, protein kinase B; COPD, chronic obstructive pulmonary disease; CSE, cigarette smoke extract; EF50, maximal expiratory flow in 50% vital capacity; EGFR, epidermal growth factor receptor; ELISA, enzyme-linked immunosorbent assay; ERK, extracellular-regulated protein kinase; GO, gene ontology; H&E, hematoxylin and eosin; IL, interleukin; KEGG, Kyoto Encyclopedia of Genes and Genomes; LPS, lipopolysaccharide; MAPK, mitogen-activated protein kinase; MU5AC, mucin-5AC; MV, minute ventilation; PBS, phosphate-buffered saline; PEF, peak expiratory flow rate; PPI, protein−protein interaction; QLT, Qilongtian capsule; QLT-H, high dose of compound Qilongtian capsule; QLT-L, low dose of compound Qilongtian capsule; QLT-M, middle dose of compound Qilongtian capsule; qRT-PCR, quantitative real-time polymerase chain reaction; Rof, roflumilast; UPLC-Q-TOF-MS/MS, ultrahigh performance liquid chromatography−quadrupole time-of-flight mass spectrometry

■ REFERENCES

(1) Ghobadi, H.; Aslani, M. R.; Hosseinian, A.; Farzaneh, E. The correlation of serum brain natriuretic peptide and interleukin-6 with quality of life using the chronic obstructive pulmonary disease assessment test. *Med. Princ Pract* **2018**, *26* (6), 509−515.

(2) Hikichi, M.; Mizumura, K.; Maruoka, S.; Gon, Y. Pathogenesis of chronic obstructive pulmonary disease (COPD) induced by cigarette smoke. *J. Thorac Dis* **2019**, *11* (Suppl. 17), S2129−S2140.

(3) King, P. T. Inflammation in chronic obstructive pulmonary disease and its role in cardiovascular disease and lung cancer. *Clin Transl Med.* **2015**, *4* (1), 68.

(4) Ehteshami-Afshar, S.; Fitzgerald, J. M.; Doyle-Waters, M. M.; Sadatsafavi, M. The global economic burden of asthma and chronic obstructive pulmonary disease. *Int. J. Tuberc Lung Dis* **2016**, *20* (1), 11−23.

(5) Sana, A.; Meda, N.; Kafando, B.; Badoum, G.; Bouland, C. Prevalence of COPD among women and relation with cooking fuel choice in Ouagadougou, Burkina Faso. *Int. J. Tuberc Lung Dis* **2020**, *24* (9), 928−933.

(6) Mathioudakis, A. G.; Vestbo, J.; Singh, D. Long-Acting bronchodilators for chronic obstructive pulmonary disease: Which One(S), how, and when? *Clin. Chest Med.* **2020**, *41* (3), 463−474.

(7) Papi, A.; Petruzzelli, S.; Vezzoli, S.; Georges, G.; Fabbri, L. M. Triple therapy for all patients with severe symptomatic COPD at risk of exacerbations. *Eur. Respir. J.* **2019**, *53* (4), 1900147.

(8) Price, D.; Henley, W.; Cancado, J.; Fabbri, L. M.; Kerstjens, H.; Papi, A.; Roche, N.; Sen, E.; Singh, D.; Vogelmeier, C. F.; et al. Risk of pneumonia in patients with COPD initiating fixed dose inhaled corticosteroid (ICS)/Long-Acting bronchodilator (LABD) formulations containing extrafine beclometasone dipropionate versus patients initiating LABD without ICS. *Pragmat Obs Res.* **2024**, *15*, 1−16.
(9) Kadushkin, A.; Tahanovich, A.; Movchan, L.; Levandovskaya, O.; Shman, T. Nortriptyline enhances corticosteroid sensitivity of blood T cells from patients with chronic obstructive pulmonary disease. *J. Physiol. Pharmacol* **2021**, *72* (5), n/a.
(10) Wu, J.; Ye, Y.; Li, C.; Zhou, W.; Chang, R. Correlation of inhaled Long-Acting bronchodilators with adverse cardiovascular outcomes in patients with stable COPD: A bayesian network Meta-Analysis of randomized controlled trials. *J. Cardiovasc Pharmacol* **2019**, *74* (3), 255−265.
(11) Zhang, J.; Zheng, J.; Huang, K.; Chen, Y.; Yang, J.; Yao, W. Use of glucocorticoids in patients with COPD exacerbations in China: A retrospective observational study. *Ther Adv. Respir Dis* **2018**, *12*, 10244627442.
(12) Goncalves, P. A.; dos Santos Neves, R.; Neto, L. V.; Madeira, M.; Guimaraes, F. S.; Mendonca, L. M. C.; Lopes, A. J.; Farias, M. L. F. Inhaled glucocorticoids are associated with vertebral fractures in COPD patients. *J. Bone Miner. Metab.* **2018**, *36* (4), 454−461.
(13) Zhang, P.; Fu, Y.; Yang, C. An Analysis of Qilongtian in Yunnan Medicine in the Treatment of Pulmonary Distension. *Henan Traditional Chinese Medicine.* **2020**, *40* (12), 1828−1830.
(14) Chen, S.-P.; Huang Liu, R.; Lu, T.-M.; Wei, J. C.-C.; Wu, T.-C.; Tsai, W.-Y.; Tsai, C.-H.; Yang, C.-C. Complementary usage of Rhodiola crenulata (L.) in chronic obstructive pulmonary disease patients: The effects on cytokines and T cells. *Phytother. Res.* **2015**, *29* (4), 518−525.
(15) Pu, W. L.; Zhang, M. Y.; Bai, R. Y.; Sun, L. K.; Li, W. H.; Yu, Y. L.; Zhang, Y.; Song, L.; Wang, Z. X.; Peng, Y. F.; et al. Anti-inflammatory effects of Rhodiola rosea L.: A review. *Biomed. Pharmacother.* **2020**, *121*, 109552.
(16) Fu, X.; Yang, C.; Chen, B.; Zeng, K.; Chen, S.; Fu, Y. Qi-Long-Tian formula extract alleviates symptoms of acute high-altitude diseases via suppressing the inflammation responses in rat. *Respir Res.* **2021**, *22* (1), 52.
(17) Chuang, M. L.; Wu, T. C.; Wang, Y. T.; Wang, Y. C.; Tsao, T. C.; Wei, J. C.; Chen, C. Y.; Lin, I. F. Adjunctive treatment with rhodiola crenulata in patients with chronic obstructive pulmonary disease-A randomized placebo controlled double blind clinical trial. *PLoS One* **2015**, *10* (6), e0128142.
(18) Hu, Y.; He, Z.; Zhang, W.; Niu, Z.; Wang, Y.; Zhang, J.; Shen, T.; Cheng, H.; Hu, W. The potential of Panax notoginseng against COVID-19 infection. *J. Ginseng Res.* **2023**, *47* (5), 622−626.
(19) Xu, Y.; Tan, H. Y.; Li, S.; Wang, N.; Feng, Y. Panax notoginseng for Inflammation-Related Chronic Diseases: A Review on the Modulations of Multiple Pathways. *Am. J. Chin Med.* **2018**, *46* (5), 971−996.
(20) Paik, S.; Song, G. Y.; Jo, E. K. Ginsenosides for therapeutically targeting inflammation through modulation of oxidative stress. *Int. Immunopharmacol.* **2023**, *121*, 110461.
(21) Lelu, J. K.; Liu, Q.; Alolga, R. N.; Fan, Y.; Xiao, W. L.; Qi, L. W.; Li, P. A new two-dimensional chromatographic method for separation of saponins from steamed Panax notoginseng. *J. Pharm. Biomed Anal* **2016**, *125*, 355−359.
(22) Liu, H. Z.; Liu, Z. L.; Zhao, S. P.; Sun, C. Z.; Yang, M. S. Protective mechanism of Panax notoginseng saponins on rat hemorrhagic shock model in recovery stage. *Cell Biochem. Biophys.* **2014**, *70* (3), 1719−1724.
(23) White, C. M.; Fan, C.; Song, J.; Tsikouris, J. P.; Chow, M. An evaluation of the hemostatic effects of hydrophilic, alcohol, and lipophilic extracts of notoginseng. *Pharmacotherapy* **2001**, *21* (7), 773−777.
(24) Wang, T.; Guo, R.; Zhou, G.; Zhou, X.; Kou, Z.; Sui, F.; Li, C.; Tang, L.; Wang, Z. Traditional uses, botany, phytochemistry, pharmacology and toxicology of Panax notoginseng (Burk.) F.H. Chen: A review. *J. Ethnopharmacol.* **2016**, *188*, 234−258.
(25) Xie, W.; Meng, X.; Zhai, Y.; Zhou, P.; Ye, T.; Wang, Z.; Sun, G.; Sun, X. Panax Notoginseng Saponins: A Review of its Mechanisms of Antidepressant or Anxiolytic Effects and Network Analysis on Phytochemistry and Pharmacology. *Molecules* **2018**, *23* (4), 940.
(26) He, B.; Chen, D.; Zhang, X.; Yang, R.; Yang, Y.; Chen, P.; Shen, Z. Oxidative Stress and Ginsenosides: An Update on the Molecular Mechanisms. *Oxid. Med. Cell. Longev.* **2022**, *2022*, 9299574.
(27) Zhang, Y.; Han, L. F.; Sakah, K. J.; Wu, Z. Z.; Liu, L. L.; Agyemang, K.; Gao, X. M.; Wang, T. Bioactive protopanaxatriol type saponins isolated from the roots of Panax notoginseng (Burk.) F. H. Chen. *Molecules* **2013**, *18* (9), 10352−10366.
(28) Yang, X.; Xiong, X.; Wang, H.; Wang, J. Protective effects of panax notoginseng saponins on cardiovascular diseases: A comprehensive overview of experimental studies. *Evid Based Complement Alternat Med.* **2014**, *2014*, 204840.
(29) Kim, M. H.; Kim, S. H.; Yang, W. M. Mechanisms of action of phytochemicals from medicinal herbs in the treatment of Alzheimer's disease. *Planta Med.* **2014**, *80* (15), 1249−1258.
(30) Yang, C.; Fu, Y.; Zhang, A.; Qi, H.; Jing, H.; Feng, Y.; Liu, Q. Effect of Qilongtian Granules on Clinical Effect and lmmune Factors in Patients with Stable COPD. *Yunnan Journal of Traditional Chinese Medicine and Materia Medica.* **2020**, *41* (11), 21−24.
(31) Liu, Q.; Fu, Y.; Yang, C.; Wu, H.; Zhang, A.; Zhang, J.; Li, J.; Jing, H. Study on the Regulation of Qilongtian on Nrf2 and DJ-1 in Chronic Obstructive Pulmonary Disease Rats. *Journal of Yunnan University of Chinese Medicine.* **2020**, *43* (04), 19−23.
(32) Ghorani, V.; Boskabady, M. H.; Khazdair, M. R.; Kianmeher, M. Experimental animal models for COPD: A methodological review. *Tob. Induc. Dis.* **2017**, *15*, 25.
(33) Zhang, L. X.; Tian, Y. G.; Zhao, P.; Feng, S. X.; Han, X. X.; Li, J. S. Network pharmacology analysis uncovers the effect on apoptotic pathway by Bu-Fei formula for COPD treatment. *J. Ethnopharmacol.* **2022**, *289*, 115022.
(34) Barnes, P. J. Cellular and molecular mechanisms of asthma and COPD. *Clin Sci. (Lond)* **2017**, *131* (13), 1541−1558.
(35) Wang, Y.; Xu, J.; Meng, Y.; Adcock, I. M.; Yao, X. Role of inflammatory cells in airway remodeling in COPD. *Int. J. Chron Obstruct Pulmon Dis* **2018**, *13*, 3341−3348.
(36) Osadnik, C. R.; Mcdonald, C. F.; Holland, A. E. Clinical issues of mucus accumulation in COPD. *Int. J. Chron Obstruct Pulmon Dis* **2014**, *9*, 301−302.
(37) Shi, L.; Yan, J.; Meng, Y.; Wang, G.; Du, J.; Feng, C. Systematic pharmacology-based strategy to explore the mechanism of bufei huoxue capsule in the treatment of chronic obstructive pulmonary disease. *Evid Based Complement Alternat Med.* **2022**, *2022*, 1129567.
(38) Ma, X.; Liu, A.; Liu, W.; Wang, Z.; Chang, N.; Li, S.; Li, J.; Hou, Y.; Bai, G. Analyze and identify peiminine target EGFR improve lung function and alleviate pulmonary fibrosis to prevent exacerbation of chronic obstructive pulmonary disease by phosphoproteomics analysis. *Front Pharmacol* **2019**, *10*, 737.
(39) Guan, S.; Xu, W.; Han, F.; Gu, W.; Song, L.; Ye, W.; Liu, Q.; Guo, X. Ginsenoside Rg1 attenuates cigarette smoke-induced pulmonary epithelial-mesenchymal transition via inhibition of the TGF-beta1/Smad pathway. *Biomed Res. Int.* **2017**, *2017*, 7171404.
(40) Guan, S.; Liu, Q.; Han, F.; Gu, W.; Song, L.; Zhang, Y.; Guo, X.; Xu, W. Ginsenoside Rg1 ameliorates cigarette smoke-induced airway fibrosis by suppressing the TGF-beta1/Smad pathway in vivo and in vitro. *Biomed Res. Int.* **2017**, *2017*, 6510198.
(41) Feng, H.; Zhang, D.; Yin, Y.; Kang, J.; Zheng, R. Salidroside ameliorated the pulmonary inflammation induced by cigarette smoke via mitigating M1 macrophage polarization by JNK/c-Jun. *Phytother. Res.* **2023**, *37* (9), 4251−4264.
(42) Luo, F.; Liu, J.; Yan, T.; Miao, M. Salidroside alleviates cigarette smoke-induced COPD in mice. *Biomed. Pharmacother.* **2017**, *86*, 155−161.

https://doi.org/10.1021/acsomega.3c10163
ACS Omega 2024, 9, 32455−32468

(43) Keshet, Y.; Seger, R. The MAP kinase signaling cascades: A system of hundreds of components regulates a diverse array of physiological functions. *Methods Mol. Biol.* **2010**, *661*, 3−38.
(44) Manley, G.; Parker, L. C.; Zhang, Y. Emerging regulatory roles of Dual-Specificity phosphatases in inflammatory airway disease. *Int. J. Mol. Sci.* **2019**, *20* (3), 678.
(45) O'Leary, L.; Sevinc, K.; Papazoglou, I. M.; Tildy, B.; Detillieux, K.; Halayko, A. J.; Chung, K. F.; Perry, M. M. Airway smooth muscle inflammation is regulated by microRNA-145 in COPD. *FEBS Lett.* **2016**, *590* (9), 1324−1334.
(46) Koga, Y.; Tsurumaki, H.; Aoki-Saito, H.; Sato, M.; Yatomi, M.; Takehara, K.; Hisada, T. Roles of cyclic AMP response element binding activation in the ERK1/2 and p38 MAPK signalling pathway in central nervous system, cardiovascular system, osteoclast differentiation and mucin and cytokine production. *Int. J. Mol. Sci.* **2019**, *20* (6), 1346.
(47) Yu, Q.; Chen, X.; Fang, X.; Chen, Q.; Hu, C. Caveolin-1 aggravates cigarette smoke extract-induced MUC5AC secretion in human airway epithelial cells. *Int. J. Mol. Med.* **2015**, *35* (5), 1435−1442.
(48) Nadel, J. A. Role of epidermal growth factor receptor activation in regulating mucin synthesis. *Respir Res.* **2001**, *2* (2), 85−89.
(49) Korfhagen, T. R.; Le Cras, T. D.; Davidson, C. R.; Schmidt, S. M.; Ikegami, M.; Whitsett, J. A.; Hardie, W. D. Rapamycin prevents transforming growth factor-alpha-induced pulmonary fibrosis. *Am. J. Respir. Cell Mol. Biol.* **2009**, *41* (5), 562−572.

https://doi.org/10.1021/acsomega.3c10163
ACS Omega 2024, 9, 32455−32468